

Vortices in the supersolid phase of dipolar Bose-Einstein condensates

Francesco Ancilotto,^{1,2} Manuel Barranco,^{3,4} Martí Pi,^{3,4} and Luciano Reatto⁵

¹*Dipartimento di Fisica e Astronomia “Galileo Galilei” and CNISM,
Università di Padova, via Marzolo 8, 35122 Padova, Italy*

²*CNR-IOM, via Bonomea, 265 - 34136 Trieste, Italy*

³*Departament FQA, Facultat de Física, Universitat de Barcelona. Av. Diagonal, 645. 08028 Barcelona, Spain*

⁴*Institute of Nanoscience and Nanotechnology (IN2UB), Universitat de Barcelona, Barcelona, Spain.*

⁵*Dipartimento di Fisica, Università degli Studi di Milano, via Celoria 16, 20133 Milano, Italy*

(Dated: April 1, 2025)

Vortices are expected to exist in a supersolid but experimentally their detection can be difficult because the vortex cores are localized at positions where the local density is very low. We address here this problem by performing numerical simulations of a dipolar Bose-Einstein Condensate (BEC) in a pancake confinement at $T = 0$ K and study the effect of quantized vorticity on the phases that can be realized depending upon the ratio between dipolar and short-range interaction. By increasing this ratio the system undergoes a spontaneous density modulation in the form of an ordered arrangement of multi-atom “droplets”. This modulated phase can be either a “supersolid” (SS) or a “normal solid” (NS). In the SS state droplets are immersed in a background of low-density superfluid and the system has a finite global superfluid fraction resulting in non-classical rotational inertia. In the NS state no such superfluid background is present and the global superfluid fraction vanishes. We propose here a protocol to create vortices in modulated phases of dipolar BEC by “freezing” into such phases a vortex-hosting superfluid (SF) state. The resulting system, depending upon the interactions strengths, can be either a SS or a NS. To discriminate between these two possible outcome of a “freezing” experiment, we show that upon releasing of the radial harmonic confinement, the expanding vortex-hosting SS shows tell-tale quantum interference effects which display the symmetry of the vortex lattice of the originating SF, as opposed to the behavior of the NS which shows instead a ballistic radial expansion of the individual droplets. Such markedly different behavior might be used to prove the supersolid character of rotating dipolar condensates.

The supersolid phase of matter has attracted large interest because the two symmetries that become spontaneously broken at the same time seem incompatible at first sight [1]. On one hand the translational symmetry is broken so that particles become localized with solid order. On the other hand gauge symmetry is broken and this leads to a condensate and to superfluid properties. Supersolidity was first proposed long ago for solid ^4He [2–4] and experiments [5] have shown that solid ^4He has indeed a number of anomalous properties but these do not conform to the bulk supersolid paradigm [5, 6]. Cold bosons turned out to be a more fruitful platform. In particular, a number of properties expected for a supersolid have recently been verified with dipolar bosons, as discussed below. In a superfluid system vortices are expected as excitations in addition to propagating phonon or phonon-roton ones. Vortices in a superfluid are quantized topological excitations directly related to an overall phase coherence of the system, so the creation and detection of quantized vortices is a fundamental verification of the basic nature of supersolidity.

A system made of dipolar bosons is very appealing in this context because, under suitable conditions, the dispersion relation of its excited states is characterized by a roton minimum –similarly to superfluid ^4He – whose gap amplitude depends on the relative strengths of short-range and dipolar interactions [7, 8]. As the ratio between dipolar interaction and short-range repulsion strength increases beyond a critical value, a spontaneous density modulation occurs which is driven by the softening of

the roton mode at finite momentum k_R , and the resulting system shows supersolid character [7, 9–13]. The density modulation, with wavelength $\sim 2\pi/k_R$, results in an ordered array of “droplets”, elongated in the direction of the polarization axis, made of many atoms each. Global phase coherence can be maintained between adjacent droplets due to a low-density superfluid background that allows tunneling of atoms from one droplet to another. Instead, when such superfluid background is absent the equilibrium phase consists of an ordered array of droplets which are essentially isolated from one another (“normal solid” phase).

Further increase in the dipolar interaction results in the formation of *self-bound* droplets [14–19], with order-of-magnitude higher densities, the binding arising from the interplay between the two-body dipolar interactions and the effect of quantum fluctuations [15, 20].

Supersolid behavior occurs in the intermediate regime between superfluid and self-bound droplets. We remark that the term droplet will be used here to indicate the individual clusters making up the ordered structure of a modulated phase in such intermediate regime, and will not refer to the self-bound droplet regime.

A number of theoretical studies predicted supersolid behavior in dipolar Bose-Einstein condensates (BEC) in different geometries, including the stripe phase when the polarization vector forms an angle with the confinement axis [9, 21, 22], dipolar gases confined in a quasi-2D pancake shaped trap [10, 16], or in a tube [12]. The order of the superfluid-supersolid transition has been studied

[1], revealing a critical point in the phase diagram where such transition becomes second-order.

There is now convincing experimental evidence of supersolid (SS in the following) behavior in dipolar gases. Strong global phase coherence was found in the SS realization of Ref. [24] as opposed to the lack of it in the isolated droplet phase where no superfluid flow is present between adjacent droplets (“normal solid”, NS in the following). Similarly, robust phase coherence across a linear array of quantum droplets was observed in Ref. [25]. Stable stripe modulations have been also observed in dipolar quantum gases [9, 26]. A partial phase coherence is suggested in Ref. [26], thus indicating possible SS behavior. The characteristic symmetry breaking of a SS phase was observed through the appearance of compressional oscillation modes in a harmonically trapped dipolar condensate [27]. In a more recent work [28] the reduction of the moment of inertia under slow rotation, previously predicted for a dipolar SS [29], has been measured. The response of the dipolar SS phase has been studied experimentally in Ref. [30] where the out-of-equilibrium superfluid (SF in the following) flow across the whole system was revealed by a rapid re-establishment of global phase coherence after a phase-shattering excitation was applied. Instead, no such re-phasing was observed in the NS phase, where tunneling between adjacent droplets is suppressed.

Most of the recent evidence of supersolid behavior in dipolar gases is based on the presence of two main features of a SS system, i.e. (i) a non-zero non-classical translational/rotational inertia [31] and (ii) the appearance of the Nambu-Goldstone gapless mode corresponding to phase fluctuations—besides the phonon mode associated to density fluctuations and resulting from the translational discrete symmetry of the system. But no evidence of another hallmark of superfluidity has been gathered so far, namely the presence of quantized vorticity [29]. Experimental realization and detection of quantized vorticity would provide a more direct evidence of global coherence in the supersolid phase of a dipolar system.

In this Rapid Communication we address the properties of vortices in the SS phase of dipolar bosons. The standard way to detect vortices in a BEC is via visualization of the density holes in the expanding condensate at the positions of the vortex cores. This procedure is likely impossible to apply in the SS state because, as shown in the following, the vortex cores are localized in the interstitial regions between droplets where the local particle density $\rho(\mathbf{r})$ is already very small, so that the additional depression of $\rho(\mathbf{r})$ at the vortex cores is almost invisible. We propose here a different protocol that will make possible to study vortices in the SS phase of dipolar BEC. We show how a procedure based on the “freezing” of the vortex-hosting SF state followed by unbinding the system from the radial trap in the plane perpendicular to the polarization axis provides a direct access to vortical states in a density-modulated dipolar system: the freezing cy-

cle allows to imprint a prescribed angular momentum in the modulated system (whether it is SS or NS), while a subsequent radial expansion allows unambiguously to discriminate if the system is in the SS or NS state.

We address the equilibrium structure and vortical excitations of a dipolar BEC confined in a pancake trap, whose short axis is parallel to the polarization direction.

A $T = 0$ dipolar BEC of atoms with mass m and magnetic moment μ is represented by a macroscopic wave function $\phi(\mathbf{r})$ that obeys the extended Gross-Pitaevskii equation (eGPE) [15]:

$$H\phi(\mathbf{r}) \equiv \left\{ -\frac{\hbar^2}{2m}\nabla^2 + V_t(\mathbf{r}) + g|\phi(\mathbf{r})|^2 + \gamma(\epsilon_{dd})|\phi(\mathbf{r})|^3 + \int d\mathbf{r}' |\phi(\mathbf{r}')|^2 V_{dd}(\mathbf{r} - \mathbf{r}') \right\} \phi(\mathbf{r}) = \varepsilon\phi(\mathbf{r}) \quad (1)$$

Here $g = 4\pi\hbar^2 a_s/m$, a_s being the s-wave scattering length, $V_{dd}(\mathbf{r}) = \frac{\mu_0\mu^2}{4\pi} \frac{1-3\cos^2\theta}{r^3}$ is the dipole-dipole interaction between two identical magnetic dipoles aligned along the z axis (θ being the angle between the vector \mathbf{r} and the polarization direction z), and μ_0 is the permeability of the vacuum. V_t is the trapping harmonic potential. The number density of the system is $\rho(\mathbf{r}) = |\phi(\mathbf{r})|^2$. The last term is the beyond-mean-field (Lee-Huang-Yang, LHY) correction [20], where $\gamma(\epsilon_{dd}) = \frac{32}{3\sqrt{\pi}}ga^{3/2}F(\epsilon_{dd})$, $\epsilon_{dd} = \frac{\mu_0\mu^2}{3g}$ being the ratio between the strengths of the dipole-dipole and contact interactions, and $F(\epsilon_{dd}) = \frac{1}{2}\int_0^\pi d\theta \sin\theta [1 + \epsilon_{dd}(3\cos^2\theta - 1)]^{5/2}$. The chemical potential ε is determined by the normalization condition $\int |\phi(\mathbf{r})|^2 d\mathbf{r} = N$, N being the total number of dipoles.

We do not find necessary to include a three-body loss term in our description of the dynamics because experimentally the density-modulated states are found to be remarkably long-lived, with a lifetime of about 150 ms [24], i.e. longer than the typical timescales investigated here.

To investigate non-zero angular momentum configurations it is convenient to move to the fixed-cloud frame of reference (co-rotating frame) by imposing a fixed value of the rotational frequency ω , i.e. we look for solutions of the equation

$$\left\{ H - \omega \hat{L}_z \right\} \phi(\mathbf{r}) = \varepsilon\phi(\mathbf{r}) \quad (2)$$

where \hat{L}_z is the total angular momentum operator.

We solve the above equations by propagating in imaginary time, if stationary states are sought, or by propagating in real-time its time-dependent counterpart $i\hbar\partial\phi/\partial t = H\phi$ to simulate the dynamics of the system. The spatial mesh spacing and time step are chosen such that during the time evolution excellent conservation of the norm, total energy and angular momentum is guaranteed. More details on how to solve these equations can be found in Ref. [12].

Our system is made by $N = 5 \times 10^5$ ^{164}Dy atoms subject to harmonic trapping potential $\omega_x = \omega_y = 40 \times 2\pi$ Hz, $\omega_z = 150 \times 2\pi$ Hz. The shape of the trapped dipolar gas is thus that of an oblate cloud, flattened in the direction of the dipole polarization (z axis).

The relative strength of the dipolar interaction over the short-range one is defined by the dimensionless parameter $\epsilon_{dd} = a_{dd}/a_s$, where $a_{dd} = 132 a_0$ is the dipolar length for ^{164}Dy atoms [30]. In the following most results are for three representative values of ϵ_{dd} , i.e. $\epsilon_{dd} = 1.33$, corresponding to the SF phase, $\epsilon_{dd} = 1.42$, corresponding to the SS phase, and $\epsilon_{dd} = 1.61$, corresponding to the NS phase. The scattering lengths associated to these values are $a_s = 99, 93$, and $82 a_0$, respectively.

We have preliminarily studied an extended system in the x - y plane, i.e. we put $\omega_x = \omega_y = 0$ and used periodic boundary conditions on a box of size $L_x = L_y = 42$ microns. Notice that in these calculations the confinement in the z direction is still present. We considered different values of ϵ_{dd} , and solved the Bogoliubov-de Gennes equations with the method described in Ref. [12]. When ϵ_{dd} is large enough the excitation spectrum develops a phonon-maxon-roton structure (see Fig. 1 in the Supplemental Material (SM)) [32]. We find that the roton gap vanishes for $\epsilon_{dd} \sim 1.35$. For larger ϵ_{dd} values the homogeneous system becomes unstable and enters the regime of self-modulated density, with a wavelength set by the wavevector at the minimum $k_R a_{ho} = 1.32$, where $a_{ho} = \sqrt{\hbar^2/m\omega_z} = 1.2112 \times 10^4 a_0$ is the harmonic length associated to the trapping potential along z ; this corresponds to a wavelength $\lambda = 2\pi/k_R = 5.8 \times 10^4 a_0$. We have also studied a vortex excitation in this extended system, with axis in the z -direction and core in the center of the box, i.e. we computed the lowest energy state for the wave function $\phi(\mathbf{r}) = \chi(\mathbf{r})\exp[i\theta]$, where χ is a real function and θ is the angular variable in the x - y plane. The conditions imposed on $\phi(\mathbf{r})$ at the boundaries of the calculation box are specified in Ref. [33]. When ϵ_{dd} is small the vortex density profile $\chi(\mathbf{r})^2$ is featureless, vanishing quadratically at the position of the vortex core as in usual BEC systems. As ϵ_{dd} is increased the density profile develops damped oscillations near the vortex core [34]. As shown in Fig. 2 of SM [32], the oscillations become more pronounced as the instability limit $\epsilon_{dd} \sim 1.35$ is approached. The wave vector of the oscillations is close to the roton k_R . These oscillations are similar to those predicted in superfluid ^4He and have been described as a cloud of virtual rotons [35].

We come now to the study of the trapped dipolar gas. We show in Fig. 1 the ground-state local density in the $z = 0$ central plane for the three studied values of ϵ_{dd} (for clarity, only the central portion of the simulation cell is shown). For $\epsilon_{dd} = 1.33$ the density is featureless and corresponds to that of a trapped SF cloud (left panel). The atom density for $\epsilon_{dd} = 1.42$ (middle panel of Fig. 1) shows that the system spontaneously develops a density modulation and the structure appears to be made of regularly arranged dipole clusters, elongated in the di-

rection of the polarization axis and immersed in a very dilute condensate background. The ratio δ between the density of this background and the maximum density of a cluster is about $\delta \sim 4.4 \times 10^{-2}$. The spatial order is that of an approximate circular portion of the triangular lattice, displaying some deformation of the cluster lattice to minimize the energy in presence of the oblate trap. Besides, the density inside the clusters diminishes as one moves towards the border of the cloud. In order to avoid possible local minima of the total energy [9, 10] we started the imaginary-time propagation from the SF state shown in Fig. 1, changing ϵ_{dd} to the appropriate value and adding some random noise (with very small amplitude) to the initial density profile. If we start instead without this preliminary randomization, we end up in a metastable structure similar to the one shown (i.e. same density modulation wavelength) but slightly different arrangement of the droplets. Such metastable states are also supersolid and are likely separated by energy barriers from the lowest energy state shown in Fig. 1.

An accepted criterion which signals a supersolid behavior is the presence, besides of a periodic, solid-like density modulation, of a finite non-classical rotational inertia (NCRI) [4, 31]. The latter is associated with the response of the system to a phase twist expressed by a global superfluid fraction f_s

$$f_s = 1 - \lim_{\omega \rightarrow 0} \frac{|\langle L_z \rangle|}{\omega I_{rb}} \quad (3)$$

where $I_{rb} = m \int \rho(\mathbf{r})(x^2 + y^2) dx dy$ is the rigid-body moment of inertia of the rotating cloud. We find $f_s = 1$ at $\epsilon_{dd} = 1.33$ and $f_s = 0.72$ at $\epsilon_{dd} = 1.42$. This verifies, respectively, the superfluid and the supersolid character of these two states. Notice that f_s should not be confused with the total superfluid fraction: for instance, in the NS phase the droplets are individually superfluid but do not contribute to the NCRI [29].

For comparison, we show in the right panel of Fig. 1 the atom density of the lowest energy state when $\epsilon_{dd} = 1.61$. We find again an ordered cluster state but in this case the halo between clusters is practically absent ($\delta \sim 10^{-5}$). This state corresponds to a NS configuration, as the calculated f_s is almost zero. Notice that the clusters appearing in the right panel of Fig. 1 (which contain up to 25,000 atoms each) are not self-bound. When one such cluster is left isolated to evolve in time in free space (i.e. without any confinement) it rapidly dilutes spreading out.

It should be noticed that the theoretical description based on the eGPE Eq. (1) is not fully appropriate for the NS because by construction the same phase is assumed for all droplets whereas in absence of the superfluid halo the phases of the droplets are uncorrelated so that a more general many-body description is in principle needed. Notwithstanding this, the description based on a single order parameter is useful because it is able to discriminate between a NS and a SS in terms of the character of the spectrum of excited states [12] built upon

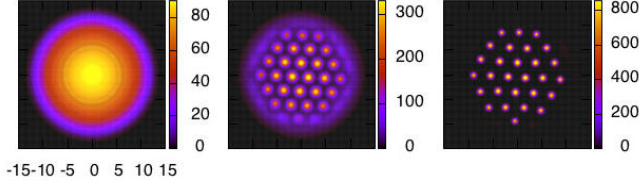


FIG. 1: Atom densities (in the plane passing through the center of the trap) for the lowest energy configurations corresponding to (from left to right) $\epsilon_{dd} = 1.33, 1.42, \text{ and } 1.61$. Lengths are in μm . The color bars show the atom densities in units of a_{ho}^{-3} .

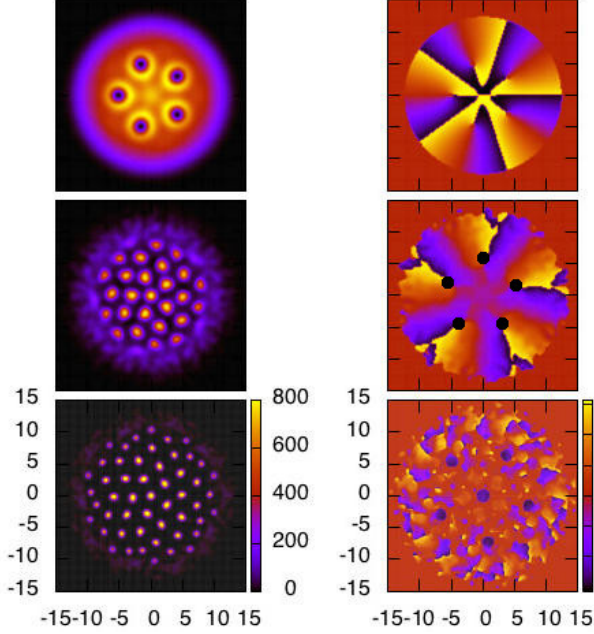


FIG. 2: Left column: atom densities of vortical states (the quantity plotted is the integrated density $\rho_{2D}(x, y) = \int \rho(x, y, z) dz$), with $\epsilon_{dd} = 1.33, 1.42, \text{ and } 1.61$ (from top to bottom). Lengths are in μm . The color bar shows the densities in units of a_{ho}^{-2} and is common to all left panels. Right column: wavefunction phase. The black dots in the middle right panel show the position of the five vortex cores in the SS phase.

the ground state and of the superfluid response that is vanishing in the NS.

To study vortical states in the SF, SS and NS configurations described above, we first produced a SF configurations hosting vortices starting from the SF ground state for $\epsilon_{dd} = 1.33$. This is easily done within the co-rotating frame using a non-zero ω value in Eq. (2). Since quantum mechanics forbids rotation of oblate SF states, in order to produce vortices the initial state has been modulated with a small quadrupolar distortion $\exp(i\epsilon xy)$, where ϵ is a small number; this could be realized experimentally by using a rotating, slightly ellipsoidal radial trap, although other methods to produce quantized vortices in dipolar SF have been proposed [36]. Using $\omega = 33$ Hz, a

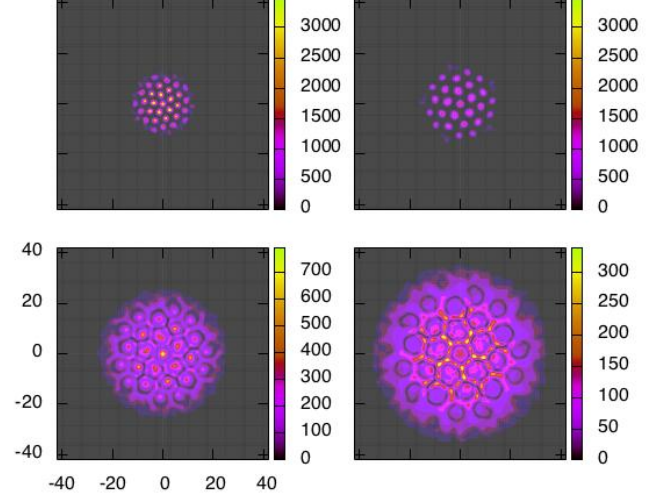


FIG. 3: Real-time expansion in the x-y plane of the SS state shown in the middle panel of Fig. 2. The four snapshots show the integrated density ρ_{2D} (in units of a_{ho}^{-2}) at times $t = 2.5, 5, 7.5, \text{ and } 10$ ms after releasing the radial trap. Lengths are in μm .

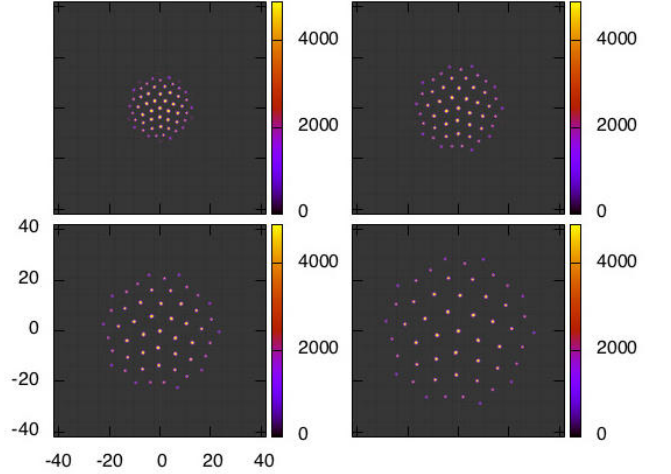


FIG. 4: Real-time expansion in the x-y plane of the NS state shown in the bottom panel of Fig. 2. The four snapshots show the integrated density ρ_{2D} (in units of a_{ho}^{-2}) at times $t = 2.5, 5, 7.5, \text{ and } 10$ ms after releasing the radial trap. Lengths are in μm .

stationary state is reached where five vortices are spontaneously nucleated. The resulting local density is shown in the top left panel of Fig. 2. One can notice the five dark spots corresponding to the vortex cores and the local density oscillations outside them similar to those found for a single vortex in the extended system. The phase of this state is shown in the top right panel of Fig. 2. The angular momentum of the rotating SF configuration is $\langle L_z \rangle = 3.33 N\hbar$. Notice that classical theory [37] predicts $\langle L_z \rangle / (N\hbar) = n_v(1 - d^2/R^2)$ for n_v linear vortices

in a rotating cylinder of radius R hosting the superfluid, all with radial distance d from the axis. Assuming the same expression, and estimating $d \sim 5.2 \mu\text{m}$ from Fig. 2, one finds $R \sim 9 \mu\text{m}$, which is comparable with the actual size of the SF cloud shown in the top left panel of Fig. 2.

We have next generated a vortical SS configuration starting from this vortex-hosting SF state by a “freezing” procedure simulated in real-time, where the scattering length a_s is linearly ramped, in 20 ms, from a value corresponding to the SF ($\epsilon_{dd} = 1.33$) to a value $\epsilon_{dd} = 1.42$ appropriate for a SS state. We then allow the system to further equilibrate in time for another 80 ms, reaching the configuration shown in the middle left panel of Fig. 2. The associated phase is displayed in the middle right panel, showing the presence of five singularities as expected for the presence of five vortices. We denote with black dots the positions of the singularities of the phase where the modulus of the wavefunction vanishes and the phase is incremented by 2π by turning around once.

The circulation calculated around a closed path encircling the central portion of the system shown in the middle panel of Fig. 2 is indeed equal to 5, and the angular momentum is the same as in the SF state. Thus, the original five vortices are still there, although it is impossible to directly image the vortex cores in this SS state because they are located in the low density region between adjacent clusters in order to minimize the energy. An expanded view of the superfluid halo between clusters is shown in Fig. 3 of SM [32].

The dynamics of nucleation of the SS phase from the SF one upon ramping the value of a_s is shown in Ref. [32]. The individual droplets initially nucleate from the vortex-induced maxima of the local density, followed by some dissociation in order to reach the correct lattice parameter. The vortices in the initial state seem thus to favor the nucleation of the cluster “crystal” and in fact vortices accelerate the SF-SS transition and the SS state is essentially reached in the ramping time of the interaction. We have also studied the SF-SS transition with the same procedure but starting from the vortex-free SF state. In this case we find a metastable structure very similar to the ground-state shown in the middle panel of Fig. 1. One can also see that in the center of the trap the local order of the clusters is different: in the 5-vortex case the clusters in the center have a five-fold coordination reflecting the order and structure of the vortices in the SF; at variance, in the freezing of the vortex-free SF the coordination is that of the triangular lattice, as visible in the middle panel of Fig. 1.

A similar freezing cycle was performed starting from the vortex-hosting SF state but ramping a_s from the value corresponding to the SF ($\epsilon_{dd} = 1.33$) up to $\epsilon_{dd} = 1.61$ appropriate for the NS state. It yielded the structure shown in the bottom left panel of Fig. 2. The local density can be very small at positions between droplets and the computation of the phase is affected by large numerical errors. Thus in the figure the phase is put to zero where the local density is below a small cut-off value.

The presence of vortices in the SS state can be inferred from the fact that the overall cluster crystal in Fig. 2 is rotating in the laboratory frame, as expected for any vortex lattice in a superfluid system. However, also the NS is rotating in the lab frame since it has been generated from the –angular momentum conserving– freezing of a SF in a rotational state. Hence, this rotation is a signature of the presence of angular momentum in the system but cannot help to distinguish a SS from a NS phase.

As a final step to distinguish between SS and NS, we perform a free expansion from the frozen configurations shown in Fig. 2 (middle and lower panels) by releasing the radial confinement (i.e. setting $\omega_x = \omega_y = 0$). Snapshots of the ensuing real-time dynamics are shown in Figs. 7 and 8. The expanding vortex-hosting SS state shows tell-tale quantum interference effects where a web of density inhomogeneities develops which reflects the 5-fold symmetry of the vortex lattice in the originating SF state, as opposed to the behavior of the NS state which shows instead a ballistic radial expansion of the individual clusters. Notice that during the expansion of the NS state the individual clusters maintain their initial size without further spreading, even if they are not self-bound states (i.e. anyone of them, left free to evolve in free space would expand like a gas). This effect is likely due to a combination of the dipole-dipole repulsion between adjacent clusters and confinement along the perpendicular direction. We checked that the expansion dynamics of SS and NS are robust against small perturbations, the expansion being almost unaffected when a small amplitude random noise is added to the phase of the initial state.

Remarkably, the density pattern developed during the later stages of the SS expansion (see last panel in Fig. 3) resembles a portion of the (metastable) honeycomb structure predicted for a dipolar supersolid at larger values of the nearest-neighbor droplet distance [1], but with a “defect” represented by the 5-fold ring visible at the center of our structure, which reflects the symmetry of the underlying vorticity field. The free expansion from a *non-rotating* SS state, shown in Fig. 4 of SM [32], also displays similar interference effects but in this case the structure is not rotating, as opposed to the case of the SS obtained by freezing the vortex-hosting SF, and the density modulations developing during the expansion represent a clean portion of the “ideal” honeycomb lattice predicted in Ref. [1].

Finally, one can rationalize the fact that upon expansion the droplets overlap and lead to interference fringes and density modulations in the SS whereas this does not happen in the NS as due to the presence (in the SS) or absence (in the NS) of the superfluid halo between droplets which acts as a glue between droplets due to the Bose statistics. The two remarkably different behaviors uncovered by our simulations, i.e. the radial expansion of a rotating SS vs. the radial expansion of a rotating NS, allow to empirically determine the nature (SS or NS) of the rotating system.

In summary, we have studied the properties of vortices

in the SS phase of dipolar bosons in a flattened oblate trap. Vorticity is created in the SS by a simple freezing procedure starting from a vortex-hosting SF cloud and subsequently ramping the scattering length characterizing the contact repulsive interaction to values where one expects the spontaneous formation of density modulated, ordered structures. If the freezing process leads to the SS state the imprinted vortices in the SF are still present in the SS and the cluster crystal is rotating. The cluster crystal is rotating also when the freezing process leads to a NS. To determine whether such rotating structures are a true SS or a NS lacking global superfluid response, we simulated a free expansion in the $x - y$ plane: the free expansion of the SS generates characteristic interference

patterns between the expanding clusters, with symmetries that reflect the geometry of the vortex lattice in the originating SF structure, whereas in the case of NS one sees a simple ballistic expansion of the clusters driven by the dipole-dipole repulsion between them.

Acknowledgments

One of us (F.A.) is indebted to Elena Poli for contributing to the early stages of this work. This work has been supported by Grant No. FIS2017-87801-P (AEI/FEDER, UE) (M.B., M.P.).

-
- [1] S. Balibar, *Nature* **464**, 176 (2010).
 - [2] A.F. Andreev and I.M. Lifshitz, *Sov. Phys. JETP* **29**, 1107 (1969).
 - [3] G.V. Chester, in *Lecture in Theoretical Physics*, ed. by K.T. Mahanthappa, W.E. Britten. (Gordon & Breach, New York, 1969); *Lecture notes of the Summer Institute for Theoretical Physics*, 1968, Boulder (CO, USA); G.V. Chester, *Phys. Rev. A* **2**, 256 (1970).
 - [4] A.J. Leggett, *Phys. Rev. Lett.* **25**, 1543 (1970).
 - [5] M.H.W. Chan, R. B. Hallock, and L. Reatto, *J. Low Temp. Phys.* **172**, 317 (2013); *J. Low Temp. Phys.* **173**, 354(E) (2013).
 - [6] M. Boninsegni and N.V. Prokof'ev, *Rev. Mod. Phys.* **84**, 759 (2012).
 - [7] L. Santos, G.V. Shlyapnikov, and M. Lewenstein, *Phys. Rev. Lett.* **90**, 250403 (2003).
 - [8] D.H.J. O'Dell, S. Giovanazzi, and G. Kurizki, *Phys. Rev. Lett.* **90**, 110402 (2003).
 - [9] M. Wenzel, F. Bottcher, T. Langen, I. Ferrier-Barbut, and T. Pfau, *Phys. Rev. A* **96**, 053630 (2017).
 - [10] D. Baillie and P.B. Blakie, *Phys. Rev. Lett.* **121**, 195301 (2018).
 - [11] L. Chomaz, R.M.W. van Bijnen, D. Petter, G. Faraoni, S. Baier, J.H. Becher, M.J. Mark, F. Wächtler, L. Santos, and F. Ferlaino, *Nature Physics* **14**, 442-446 (2018).
 - [12] S.M. Roccuzzo and F. Ancilotto, *Phys. Rev. A* **99**, 041601(R) (2019).
 - [13] Y. Kora and M. Boninsegni, *J. Low Temp. Phys.* **197**, 337 (2019).
 - [14] M. Schmitt, M. Wenzel, F. Bottcher, I. Ferrier-Barbut, and T. Pfau, *Nature* **539**, 259 (2016).
 - [15] F. Wächtler and L. Santos, *Phys. Rev. A* **93**, 061603(R) (2016).
 - [16] D. Baillie, R.M. Wilson, R.N. Bisset, and P.B. Blakie, *Phys. Rev. A* **94**, 021602(R) (2016).
 - [17] L. Chomaz, S. Baier, D. Petter, M.J. Mark, F. Wachtler, L. Santos, and F. Ferlaino, *Phys. Rev. X* **6**, 041039 (2016).
 - [18] H. Kadau, M. Schmitt, M. Wenzel, C. Wink, T. Maier, I. Ferrier-Barbut, and T. Pfau, *Nature* **530**, 194 (2016).
 - [19] I. Ferrier-Barbut, H. Kadau, M. Schmitt, M. Wenzel, and T. Pfau, *Phys. Rev. Lett.* **116**, 215301 (2016).
 - [20] A.R.P. Lima and A. Pelster, *Phys. Rev. A* **84**, 041604(R) (2011).
 - [21] R. Bombin, J. Boronat, and F. Mazzanti, *Phys. Rev. Lett.* **119**, 250402 (2017).
 - [22] F. Cinti and M. Boninsegni, *Phys. Rev. A* **96**, 013627 (2017).
 - [23] Y.-C. Zhang, F. Maucher, and T. Pohl, *Phys. Rev. Lett.* **123**, 015301 (2019).
 - [24] L. Chomaz, D. Petter, P. Ilzhöfer, G. Natale, A. Trautmann, C. Politi, G. Durastante, R.M.W. van Bijnen, A. Patscheider, M. Sohmen, M.J. Mark, and F. Ferlaino, *Phys. Rev. X* **9**, 021012 (2019).
 - [25] F. Böttcher, J.-N. Schmidt, M. Wenzel, J. Hertkorn, M. Guo, T. Langen, and Tilman Pfau, *Phys. Rev. X* **9**, 011051 (2019).
 - [26] L. Tanzi, E. Lucioni, F. Fama, J. Catani, A. Fioretti, C. Gabbanini, R.N. Bisset, L. Santos and G. Modugno, *Phys. Rev. Lett.* **122**, 130405 (2019).
 - [27] L. Tanzi, S. M. Roccuzzo, E. Lucioni, F. Fama, A. Fioretti, C. Gabbanini, G. Modugno, A. Recati, and S. Stringari, *Nature* **574**, 382 (2019).
 - [28] L. Tanzi, J.G. Maloberti, G. Biagioni, A. Fioretti, G. Gabbanini, and G. Modugno, *arXiv:1912.01910* (2019).
 - [29] S.M. Roccuzzo, A. Gallemi, A. Recati, and S. Stringari, *Phys. Rev. Lett.* **124**, 045702 (2020).
 - [30] P. Ilzhöfer, M. Sohmen, G. Durastante, C. Politi, A. Trautmann, G. Morpurgo, T. Giamarchi, L. Chomaz, M. J. Mark, and F. Ferlaino, *arXiv:1912.10892* (2019).
 - [31] Y. Pomeau and S. Rica, *Phys. Rev. Lett.* **72**, 2426 (1994); N. Sepulveda, C. Josserand, and S. Rica, *Eur. Phys. J. B* **78**, 439-447 (2010).
 - [32] See Supplemental Material at [URL will be inserted by publisher] for additional informations and for movies showing the real-time dynamics of the processes described by Figs. 2, 3 and 4.
 - [33] M. Pi, R. Mayol, A. Hernando, M. Barranco, and F. Ancilotto, *J. Chem. Phys.* **126**, 244502 (2007).
 - [34] S. Yi and H. Pu, *Phys. Rev. A* **73**, 061602(R) (2006).
 - [35] I. Amelio, D.E. Galli, and L. Reatto, *Phys. Rev. Lett.* **121**, 015302 (2018).
 - [36] F. Malet, T. Kristensen, S.M. Reimann, and G.M. Kavoulakis, *Phys. Rev. A* **83**, 033628 (2011); S. B. Prasad, T. Bland, B.C. Mulkerin, N.G. Parker, and A.M. Martin, *arXiv:1906.08664v2* (2019).
 - [37] G.B. Hess, *Phys. Rev.* **161**, 189 (1967).

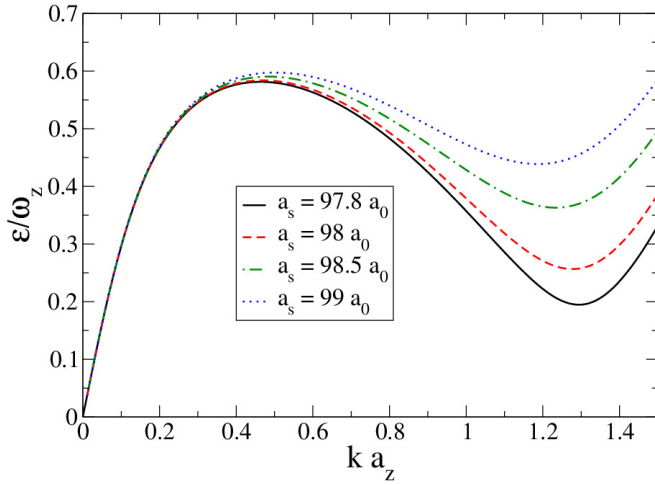


FIG. 5: Dispersion relations of the extended system for different values of a_s . Energies are in units of the harmonic energy ω_z and wavevectors are in units of the inverse of the harmonic length $a_z = \sqrt{\hbar/(m\omega_z)}$.

Supplemental Material

We show in Fig. 5 the excitation spectrum of the extended system, i.e. subject to the harmonic confinement along the z -axis but uniform in the $x - y$ plane, for values of a_s close to the threshold for the density instability leading to the supersolid phase. The four curves represent the excitation spectrum for $a_s = 97.8, 98, 98.5$, and $99 a_0$, which correspond to a narrow range of values of ϵ_{dd} between $\epsilon_{dd} = 1.35$ (corresponding to $a_s = 97.8 a_0$) and $\epsilon_{dd} = 1.33$ (corresponding to $a_s = 99 a_0$). The vanishing of the roton gap occurs just below $a_s = 97.8 a_0$.

We show in Fig. 6 the calculated equilibrium density profiles of singly-quantized vortices in the extended system for the same values of a_s used in Fig. 5. The higher the density peaks around the vortex core, the lower the corresponding value of a_s .

An expanded top view of the superfluid halo between clusters in the rotating SS structure discussed in the main text is shown in Fig. 7, obtained by plotting the density in the $z = 0$ central plane within a narrow range of values ($\sim 1\%$ of the maximum density in the clusters). Notice the very distorted and asymmetric vortex cores, as also found in Ref. [2].

Fig. 8 shows the free expansion (i.e. setting $\omega_x = \omega_y = 0$, but keeping the confinement along the z -direction) of the SS state generated from the SF state without vortices. The quantity plotted is the integrated density

$\rho_{2D}(x, y) = \int \rho(x, y, z) dz$. Notice the interference effects due to the presence of the SF background. During the time evolution the structure appears to be non-rotating, as opposed to the case of the SS obtained from the SF with vortices. During the expansion (see the bottom right panel of Fig. (8)) the density shows temporarily the typical honeycomb structure which is predicted to be a (metastable) supersolid phase of dipolar BEC for

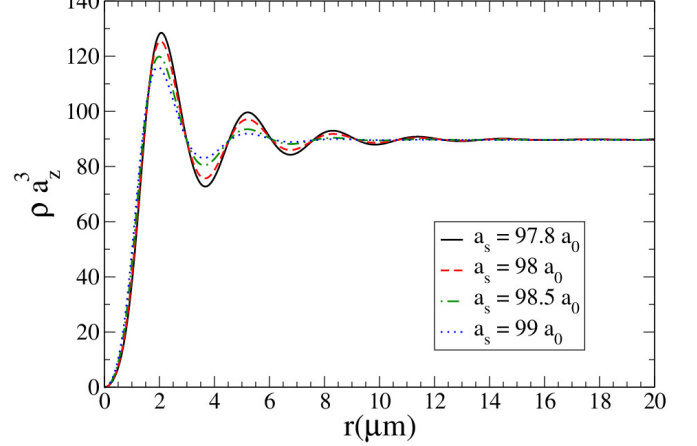


FIG. 6: Radial density profiles for a vortex in the extended system for different values of a_s .

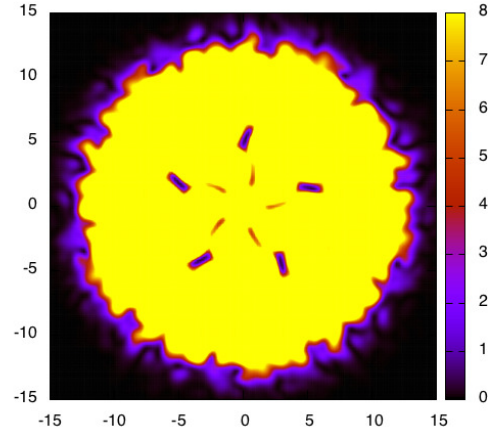


FIG. 7: Low density plot (in units of a_{ho}^{-3}) in the $z = 0$ plane for the SS phase with vorticity. Lengths are in μm .

larger values of the “lattice constants” (i.e. the nearest-neighbor cluster distance [1]).

-
- [1] Y.-C. Zhang, F. Maucher, and T. Pohl, Phys. Rev. Lett. **123**, 015301 (2019).
 [2] S.M. Roccuzzo, A. Gallemi, A. Recati, and S. Stringari,

Phys. Rev. Lett. **124**, 045702 (2020).

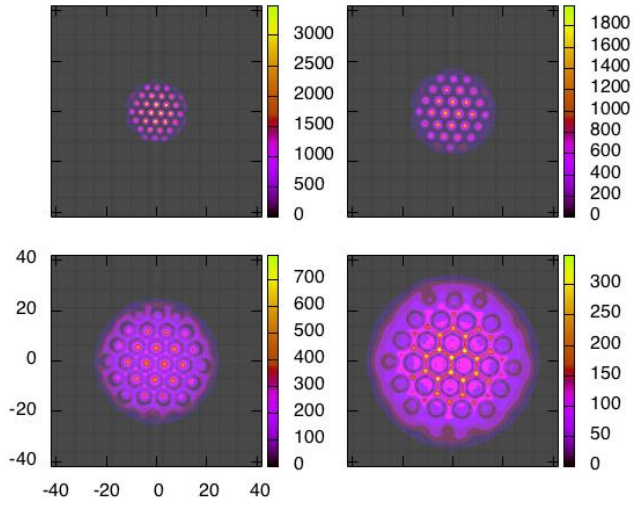


FIG. 8: Expansion of the non-rotating supersolid phase with $\epsilon_{dd} = 1.42$. The four snapshots show the integrated density ρ_{2D} (in units of a_{ho}^{-2}) at times $t = 2.5, 5, 7.5$, and 10 ms after releasing the radial trap. Lengths are in μm , and the scale is common to all panels.